JPhys Energy

OPEN ACCESS

RECEIVED
30 October 2019

REVISED
5 January 2020

ACCEPTED FOR PUBLICATION
8 January 2020

PUBLISHED
10 February 2020

PAPER

On efficiency of earth-abundant chalcogenide photovoltaic materials buffered with CdS: the limiting effect of band alignment

Elaheh Ghorbani

Fachgebiet Materialmodellierung, Institut für Materialwissenschaft, TU Darmstadt, Otto-Berndt-Straße 3, D-64287 Darmstadt, Germany

E-mail: ghorbani@mm.tu-darmstadt.de

Keywords: earth-abundant chalcogenides, band alignment, buffer/absorber interface, first-principles calculations

Abstract

Earth-abundant and environmentally-friendly Cu_2–II–IV–VI_4 (II = Sr, Ba; IV = Ge, Sn; VI = S,Se) are considered materials for the absorber layers in thin film solar cells. Attempts to understand and improve optoelectronic properties of these newly emerged absorbers resulted in an efficiency of 5.2% in less than two years. However, the energy band alignment at the buffer/absorber interface has not been studied yet; an information which is of crucial importance for designing high performance devices. Therefore, current study focuses on the band offsets between these materials and the CdS buffer. Using first-principles calculations, band discontinuities are calculated at the buffer/absorber interface. The results yield a type-II band alignment between all Cu_2–II–IV–VI_4 absorbers and CdS, hence a negative ΔE_c. Adoption of a negative ΔE_c (cliff-like conduction band offset) at the buffer/absorber interface, however, gives rise to low open circuit voltage and high interface-related recombinations. Therefore, it is necessary to search for an alternative buffer material that forms a type-I band alignment with these absorbers, where the conduction band minimum and the valence band maximum are both localized on the absorber side.

1. Introduction

$Cu(In,Ga)(S,Se)_2$ (CIGS) with the world record efficiency of 22.9% [1] is a promising material for thin film solar cells. However, In and Ga are expensive elements, which limit the manufacturing capacity of CIGSe-based solar cells. In this context, $Cu_2ZnSn(S, Se)_4$ (CZTS)—with Zn and Sn on the III^+ cation sites—received a lot of scientific attention. In 1997, Katigiri *et al* fabricated a photovoltaic cell with CZTS film and reported a conversion efficiency of 0.66% [2]. This value raised to 12.6% efficiency in 2013 [3]. Despite this significant improvement, the record value is still far below the efficiency limit of single-junction solar cells. The low conversion efficiency was found to originate from low open circuit voltage (V_{OC}) of these devices [4, 5]. The voltage deficit is assigned to the formation of band-edge tail states, which stem from the formation of copper-on-zinc and zinc-on-copper antisites [6, 7].

For avoiding the limiting effects of antisite disordering, in 2016, Shin *et al* [8] suggested to replace Cu–Zn combinations by chemically less similar elements, a new class of earth-abundant materials with chemical formula I_2–II–IV–VI_4: I accounts for Ag or Cu, II accounts for Sr or Ba, IV accounts for Sn or Ge, and VI accounts for S or Se. In 2017, Xiao *et al* used density functional theory (DFT) to study the formation energy of intrinsic defects in $Cu_2BaSnSe_4$, as a case study for this new class of materials [9]. Their study revealed that the cation-on-cation antisites such as Ba-on-Cu and Cu-on-Ba have high formation energies and are very unlikely to form at all growth conditions [9]. Hence, these new chalcogens will not suffer from large antisite-related V_{OC} deficits (as seen in CZTS). In the same year, Shin *et al* reported a conversion efficiency of 5.2% for $Cu_2BaSnS_{4-x}Se_x$ based solar cells, which demonstrated their rapid development [10]. To further optimize the performance of these new photovoltaic materials, however, details on their electronic band alignment at the buffer/absorber interface is necessary.

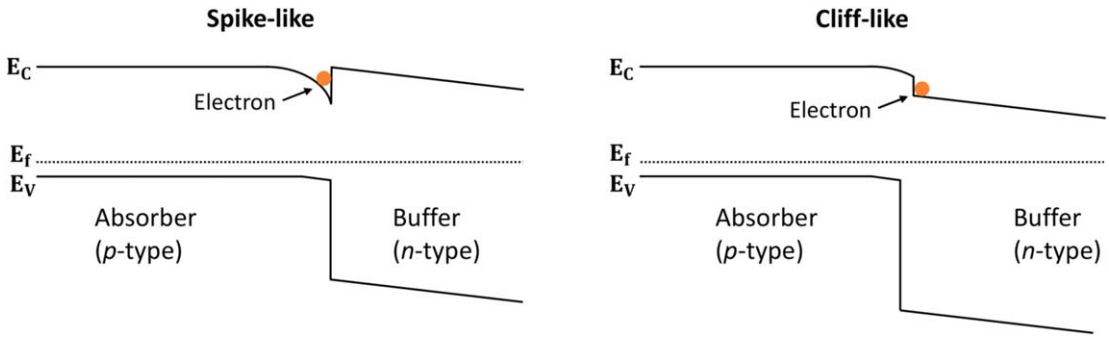

Figure 1. A simplified schematic of spike-like and cliff-like conduction band conformations at the *pn*-junction.

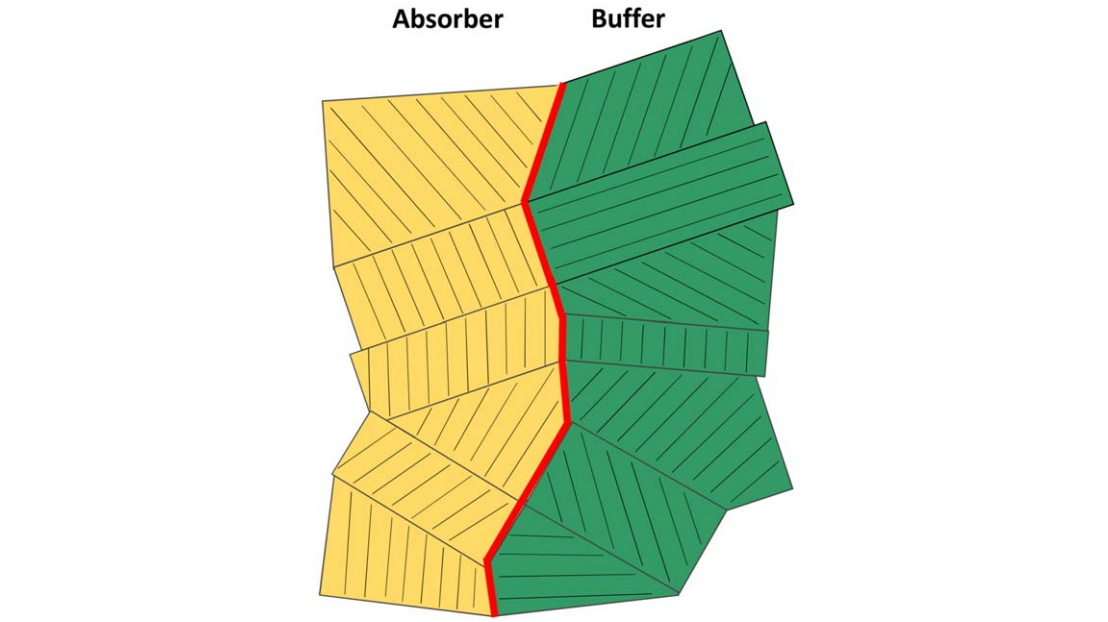

Figure 2. Conceptual schematic of buffer/absorber interface in polycrystalline thin film solar cells.

Conduction bands of absorber and buffer are either aligned, i.e. no offset exists, or discontinuous. In the latter case, if the conduction band of the absorber is below that of the buffer, a spike-like discontinuity forms (figure 1, left). And if the conduction band of the absorber is above that of the buffer, a cliff-like discontinuity forms (figure 1, right). While a moderate spike-like offset (0.0–0.3 eV) suppresses charge recombination, a cliff-like offset triggers recombination and reduces the interface band gap [11]. Thus, cliff-like conduction band offset must be avoided.

To obtain electronic band alignment between two semiconductors, their energy levels need to be aligned with respect to a common reference level [12–19]. In general, an accurate calculation of band alignment requires both bulk and interface calculations. However, interface calculations are usually hindered by several factors. First, the lack of knowledge on orientation relationships between two compounds present at the interface. In this case, supercell calculations are typically done for some lattice matched orientations, which might not exist in real samples. Second, even for the experimentally known interface orientations, modelling the interface requires performing calculations for large supercells, which are computationally very expensive. Third, absorber materials in thin film solar cells are commonly grown as polycrystalline thin films, where each grain can orient differently close to the interface. Therefore, different interface orientations exist across the interface and calculations on a specific interface orientation represent only a small part of the real-system interface. A conceptual schematic of buffer/absorber interface in polycrystalline films is shown in figure 2.

In this paper, calculations are presented on copper-based chalcogenide (CBC) compounds (the Ag-based chalcogenides are not studied here). Band alignments are discussed between $Cu_2BaSnSe_4$, $Cu_2BaGeSe_4$, $Cu_2SrGeSe_4$, $Cu_2SrSnSe_4$, Cu_2BaSnS_4, Cu_2BaGeS_4, Cu_2SrGeS_4, Cu_2SrSnS_4 absorbers and the CdS buffer. First, the energy levels of the studied materials were aligned with respect to their bulk core level energies. Then, to

investigate the effect of interfaces on the calculated bulk band alignments, supercell calculations were done for $Cu_2BaSnSe_4$/CdS (001) interface, as a case study. The obtained results show small deviations from bulk lineups.

2. Calculation methods

All calculations were done within the framework of DFT using the Vienna *ab-initio* simulation package [24, 25]. Bulk calculations were done using the range-separated Heyd–Scuseria–Ernzerhof (HSE) hybrid functional with a mixing parameter of $\alpha = 0.25$. The exchange-screening length w was set to 0.13 and 0.10 $Å^{-1}$ for CBCs and CdS, respectively [26]. This choice of screening parameters produces an accurate band gap for each material. A plane-wave cutoff energy of 400eV was applied for all calculations. Ionic positions were allowed to relax until residual forces were below 10 meV $Å^{-1}$. Γ-centered k-point grids of $2 \times 2 \times 4$, $6 \times 6 \times 2$, and $8 \times 8 \times 8$ were used for sampling Brillouin zones of tetragonal CBCs, trigonal CBCs, and CdS, respectively. The calculated bulk properties of CBCs are listed in table 1 and their crystal structures are shown in figure 3. For CdS, the calculated lattice parameter and electronic band gap are respectively 5.88 Å and 2.43 eV, in agreement with experiment [27, 28].

Using core level energies, valence band offset at the X/Y interface can be obtained by

$$\Delta E_v(X/Y) = \Delta E_{v,c'}(Y) - \Delta E_{v,c}(X) + \Delta E_{c,c'}(X/Y), \quad (1)$$

where $\Delta E_{v,c}(X)$ and $\Delta E_{v,c'}(Y)$ represent the energy separation between valence band maximum (VBM) and core level energy of the bulk buffer (X) and absorber (Y), respectively. $\Delta E_{c,c'}(X/Y)$ is the energy difference between core levels of the X and Y compounds at the X/Y interface. The conduction band offsets can be then calculated using the relation

$$\Delta E_c(X/Y) = E_g^X - E_g^Y - \Delta E_v(X/Y), \quad (2)$$

where E_g^X and E_g^Y are the band gaps of buffer and absorber, respectively.

In current calculations, the energy of the Cu 2p state was used for aligning the energy levels of the CBC compounds, while the energy band alignment between CdS and CBTS was calculated with respect to the energy of S 2s core state. The values of valence band offset and conduction band offset between other absorber materials and CdS were derived by making use of the transitivity rule

$$\Delta E_v(X/Y) = \Delta E_v(X/Z) - \Delta E_v(Y/Z), \quad (3)$$

where X, Y, and Z represent CdS, CBC compound, and CBTS, respectively. Note that valence band offset becomes positive when the VBM of CdS with respect to core level is lower than that of CBC, and conduction band offset becomes negative, when the conduction band minimum (CBM) of CdS with respect to the common core level is below that of CBC.

So-far, no experimental report is available on the interface orientation between CBCs and CdS. Therefore, alignments based on core level energies are bulk-intrinsic lineups and the energy separation between core levels of X and Y compounds at the X/Y interface (i.e. the $\Delta E_{c,c'}(X/Y)$ term in equation (1)) was not considered in these calculations. However, to check the influence of the interface on calculated band alignments, supercell calculations were performed for the CdS/CBTSe heterojunction, as a case study. At this part, to obtain band offsets, first, separate electronic band-structure calculations were performed for CdS and CBTSe in their equilibrium geometry, using the HSE hybrid functional. The VBM and CBM were determined with respect to the average electrostatic potentials of the respective bulk material. Then, explicit interface calculations were performed to obtain the alignment of the average electrostatic potential between the two materials at the interface. The supercell calculations were performed using the semi-local generalized gradient approximation of Perdew, Burke and Ernzerhof (PBE) [29]. The Brillouine zone was sampled with Γ-centered k-point mesh of $3 \times 3 \times 1$. To gain insights on the influence of interfacial strain on lineups, three differently strained CdS/CBTSe (001) supercells were considered in this study. Further details on this part of calculations are given in section 3.2.

3. Results and discussions

3.1. Band alignments based on bulk core level energies

Figure 4 shows the calculated band alignment of CBC absorbers and CdS buffer with respect to the VBM and CBM of Cu_2BaSnS_4. Using the transitivity rule, the values of valence and conduction band offsets were calculated between different CBCs and CdS and are listed in table 2. A comparison between compounds with common cations and different anions (i.e. CBTS versus CBTSe; CBGS versus CBGSe; CSGS versus CSGSe; or CSTS versus CSTSe) shows that by increasing the atomic number of the anion from S to Se, the VB moves slightly upward while the CB moves downward, resulting in a decreased band gap. The upper valence band of all

Table 1. Equilibrium lattice constants (a, b and c), band gap energy (E_g), crystal structure, and space group (SG) of the CBC materials. Lattice constants and band gaps were calculated using the HSE functional. Experimentally reported values are given in parentheses.

	Cu_2BaSnS_4 (CBTS)	$Cu_2BaSnSe_4$ (CBTSe)	Cu_2BaGeS_4 (CBGS)	$Cu_2BaGeSe_4$ (CBGSe)	Cu_2SrGeS_4 (CSGS)	$Cu_2SrGeSe_4$ (CSGSe)	Cu_2SrSnS_4 (CSTS)	$Cu_2SrSnSe_4$ (CSTSe)
a (Å)	6.40 (6.37 [8])	11.13 (11.11 [8])	6.25 (6.21 [20])	6.55 (6.50 [21])	6.16 (6.14 [20])	10.82 (10.81 [21])	6.32 (6.29 [22])	11.01 (10.97 [23])
b (Å)	5.54 (6.37 [8])	11.34 (11.23 [8])	5.41 (6.21 [20])	5.67 (6.50 [21])	5.33 (6.14 [20])	10.78 (10.74 [21])	5.46 (6.29 [22])	10.84 (10.75 [23])
c (Å)	15.84 (15.83 [8])	6.78 (6.70) (6.74 [8])	15.55 (15.53 [20])	16.32 (16.36 [21])	15.29 (15.28 [20])	6.56 (6.54 [21])	15.58 (15.57 [22])	6.73 (6.70 [23])
E_g (eV)	2.00 (1.95 [8])	1.84 (1.72 [8])	2.69	1.89	2.73	2.03	1.99 (1.90 [23])	1.75 (1.50 [23])
Structure	Trigonal	Tetragonal	Trigonal	Trigonal	Trigonal	Tetragonal	Trigonal	Tetragonal
SG	$P3_1$	Ama2	$P3_1$	$P3_1$	$P3_2$	Ama2	$P3_1$	Ama2

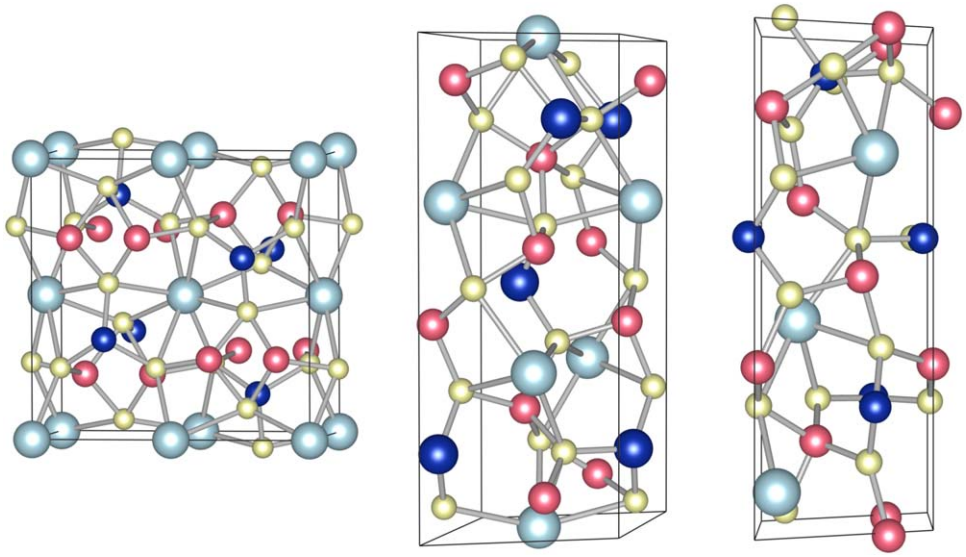

Figure 3. Crystal structures of compounds of space group *Ama*2 (left), $P3_1$ (middle), and $P3_2$ (right). The group I (Cu), II (Sr/Ba), IV (Ge/Sn), and VI (S/Se) atoms are shown in pink, light blue, dark blue, and yellow, respectively.

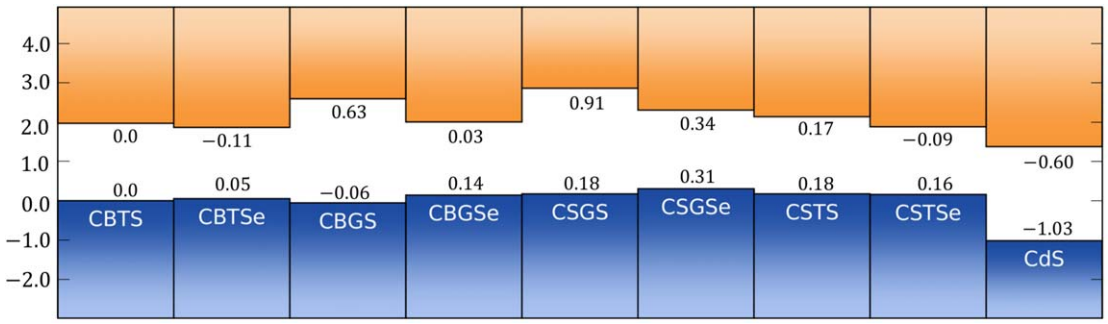

Figure 4. Calculated band lineups of bulk materials. For each material, the lower and upper numbers indicate, respectively, the position of VBM and CBM with respect to CBTS in eV.

Table 2. Calculated values of valence and conduction band offsets between different absorber materials and CdS.

	CBTS	CBTSe	CBGS	CBGSe	CSGS	CSGSe	CSTS	CSTSe
Valence band offset (eV)	1.03	1.08	0.97	1.17	1.21	1.34	1.21	1.19
Conduction band offset (eV)	−0.60	−0.49	−1.23	−0.63	−1.51	−0.94	−0.77	−0.51

CBC compounds consist of a strong hybridization between Cu *d* and S/Se *p* orbitals. The 4*p* orbital of Se is higher in energy than the 3*p* orbital of S, therefore VBM of selenides are expected to be markedly higher than sulfides. For instance, the VBM of ZnSe is 0.52 eV higher than that of ZnS [30]. In CBCs, similar to chalcopyrites [31] and Kesterites [32], the valence band offset between selenides and sulfides is small. This feature is attributed to existence of $p - d$ repulsion in these materials. Therefore, due to shorter Cu–S bond length (compared to Cu–Se bond length), the $p - d$ repulsion is stronger in sulfides, thus the valence band of sulfides are pushed upward more strongly. As a consequence, the valence band offset between Cu-based sulfides and selenides is small.

Figure 4 shows that replacing Sn with Ge shifts the CBM to higher energies, while the VBM remains less affected. Note that in sulfides, CBM of Sn-based compounds (i.e. CBTS and CSTS) are considerably lower than that of Ge-based ones (i.e. CBGS and CSGS). In selenides, however, the conduction band offset between Sn-based (i.e. CBTSe and CSTSe) and Ge-based (i.e. CBGSe and CSGSe) compounds are small. The CBM states of CBCs have the antibonding character of Sn/Ge *s* and S/Se *s* hybridization. Note that sequence of IV–VI bond length is as: Ge–S < Ge–Se < Sn–S < Sn–Se. Therefore, due to the shorter IV–VI bond length in CBGS, CBGS

has a stronger *s–s* hybridization, and consequently its CBM is positioned higher in energy relative to CBTS, CBGSe, and CBGS. This feature suggests a more negative conduction band offset between the Ge-containing absorbers and buffer materials. In consequence, the V_{OC} of Ge-based CBC absorbers is expected to be considerably lower than that of the Sn-based ones.

As mentioned, to achieve the best device performance, conduction band offset needs to be moderately positive (spike-like) at the *pn*-junction. However, as illustrated in figure 4 and shown in table 2, band alignments between all CBCs and CdS are of type-II: The CBM is localized on the CdS buffer, while the VBM is on the absorber materials. Thus, potential change at the interface is cliff-like ($\Delta E_c < 0$). At a cliff-like conduction band offset, the injected electrons coming from a forward bias face a barrier at the buffer/absorber interface and recombination between majority charge carriers increases via defects present at the interface. As a result, the V_{OC} decreases and the interface-dominated recombination increases [11, 33].

In 2017, Shin *et al* reported an efficiency of 5.2% for Selenized CBTS [10]. Despite their significant achievement, the reported V_{OC} of their device was very low (around 610mV). Soon afterward, Ge *et al* [34] deposited oxygenated CdS (CdS:O) on CBTS absorber and increased the V_{OC} by 450mV. Considering lower electron affinity of CdS:O compared to CdS, they suggested formation of a cliff-like conduction band offset as the key-factor in the V_{OC} deficit of CdS-buffered devices, which is in agreement with present results. Therefore, to enhance V_{OC} and conversion efficiency in CBC-based thin films, the conventional CdS buffer layer should be replaced by an alternative buffer material, which forms a type-I band alignment with these absorbers: The CBM and the VBM are both localized on the absorber side. Due to the toxicity of Cd, search for an alternative buffer material is also encouraged by environmental reasons.

3.2. Band alignments based on average electrostatic potential

To examine the effect of the interface on band alignment, supercell calculations were done for the CdS/CBTSe heterojuction, as a case study. The CdS/CBTSe supercell is constructed from conventional unit cells of CBTSe and CdS in (001) direction. The optimized bulk lattice parameters were $a = 11.13$ Å, $b = 11.35$ Å, $c = 6.78$ Å for CBTSe and $a = 5.88$ Å for CdS. In this study, a 2×2 unit of CdS (001) was placed on top of the CBTSe (001) surface. With this construction, the lattice mismatch at the interface is about 5%. The termination studied here is cation-terminated CdS and anion-terminated CBTSe, where Cd ions at the interface are tetrahedrally bonded to anions and the Se ions are five-fold bonded to the cations. Other possible terminations are (1) anion-terminated CdS and CBTSe, which contains anion-anion bonds, (2) cation-terminated CdS and CBTSe, which contains cation-cation bonds, and (3) anion-terminated CdS and cation-terminated CBTSe, which contains anion-cation bonds. The first two terminations have obviously large interface energy due to large density of wrong bonds at the interface. In the latter termination, i.e. anion-terminated CdS and cation-terminated CBTSe, the electronic distribution at the interface will be more distorted than the one studied here. This is because the chemical environment of three chemically different cations (i.e. Cu, Ba, and Sn) will be distorted, which results in higher interface dipoles. Considering different bonding environments at the interface, the cation-terminated CdS and anion-terminated CBTSe termination is energetically the most favorable one. Therefore, instead of considering different interface terminations, different strain conditions at the interface were studied here.

To investigate the effect of strain on band lineups, three differently strained supercells were constructed. One in which CBTSe layer is unstrained and CdS layer is strained to in-plane lattice constant of CBTSe—that is, $a_{||} = 11.13$ Å and $b_{||} = 11.35$ Å. One other in which CdS is unstrained and CBTSe is strained to the in-plane lattice constants of CdS—that is, $a_{||} = b_{||} = 11.76$ Å. And one between the two boundary cases, i.e. the in-plane lattice constants are the average of those of CBTSe and CdS—that is, $a_{||} = 11.45$ Å and $b_{||} = 11.56$ Å. To reach bulk-like region on both sides of the interface, the constructed supercells contain seven and eight layers of CBTSe and CdS, respectively. This amounts to 480 ions in each configuration, and a length of 93.59 Å along [001] direction.

Here, the alignments were calculated using the macroscopic average of the electrostatic potential of the CdS/CBTSe heterostructure. First, the planar average of the electrostatic potential along the CdS/CBTSe interface ($\overline{V}(z)$) was calculated using the expression:

$$\overline{V}(z) = \frac{1}{A}\int V(\bar{r})\,dxdy, \tag{4}$$

where A represents the area of the interface. This planar-averaged potential exhibits periodic oscillations along the [001] direction. To remove the oscillations, the macroscopic average potential $\overline{\overline{V}}(z)$ was obtained as follows

$$\overline{\overline{V}}(z) = \frac{1}{L}\int_{-L/2}^{+L/2} \overline{V}(z)\,dz, \tag{5}$$

where L is the length of the period of oscillation perpendicular to the interface. Then, the valence band offset was obtained using

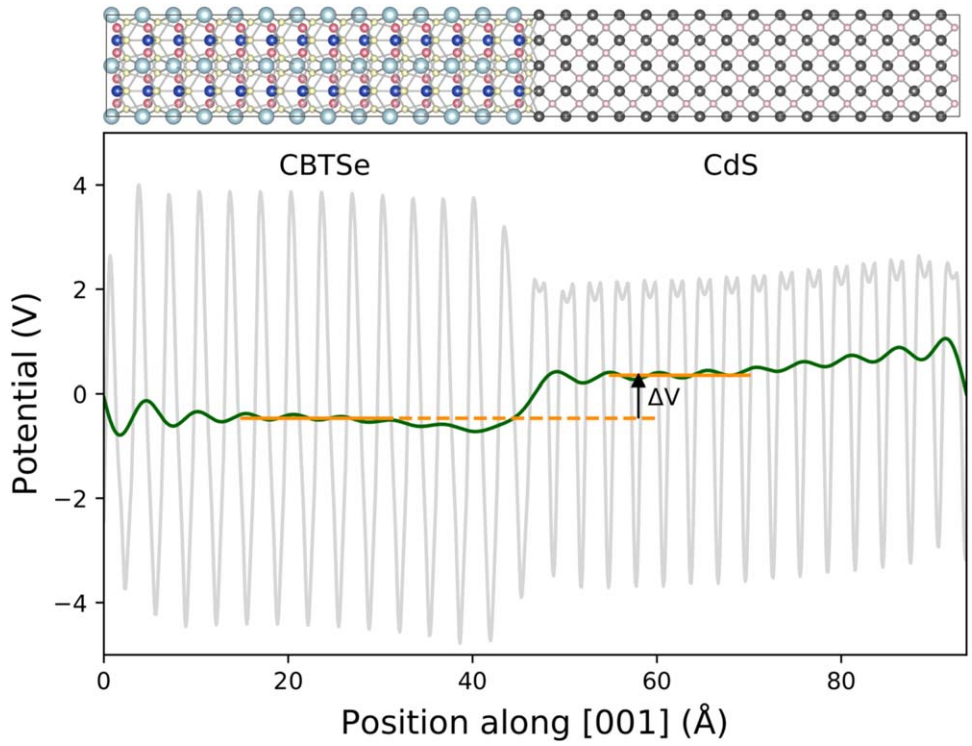

Figure 5. Top: Atomic structure of a (001)-oriented CdS/CBTSe heterojunction, where CBTSe layer is unstrained and CdS is strained to in-plane lattice parameters of CBTSe. Cu, Ba, Sn, Se, Cd and S atoms are shown in pink, light blue, dark blue, yellow, dark gray, and light pink spheres, respectively. Bottom: Planar-averaged (grey line) and macroscopically averaged (green line) electrostatic potential of the corresponding supercell.

Table 3. The in-plane lattice parameters ($a_{||}$ and $b_{||}$) for different strain conditions, as denoted in the text. Potential alignment ΔV, valence band offset (ΔE_v), and conduction band offset (ΔE_c) are presented for differently strained CdS/CBTSe supercells.

$a_{\|\|}$ (Å)	$b_{\|\|}$ (Å)	ΔV (eV)	ΔE_v (eV)	ΔE_c (eV)
11.13	11.35	0.82	1.09	−0.50
11.45	11.56	0.78	1.13	−0.54
11.76	11.76	0.75	1.16	−0.57

$$\Delta E_v = (E_v^{CdS} - E_v^{CBTSe}) + \Delta V, \tag{6}$$

where E_v^{CBTSe} (E_v^{CdS}) represents the position of the VBM with respect to the average electrostatic potential in CBTSe (CdS) bulk materials. ΔV represents potential alignment obtained from difference between values of $\overline{\overline{V}}(z)$ of CdS and CBTSe at the interface (figure 5).

In a recent study, Weston *et al* [35], proposed an accurate and computationally efficient methodology for calculating band alignment at semiconductor interfaces. According to Weston *et al* [35], values of ΔV obtained from semi-local functional are in a very good agreement with those obtained from HSE functional. Therefore, while E_v^{CBTSe} and E_v^{CdS} are obtained from bulk band-structure calculations using HSE functional, ΔV can be safely obtained from supercell calculations using PBE functional. This combined methodology produces accurate band alignment at a reasonable computational cost.

Table 3 shows results of CdS/CBTSe heterostructure, for different strain conditions (as specified by $a_{||}$ and $b_{||}$). The calculated band lineups show a small dependence upon strain situation of the system (within 70 meV). Note that the lineups for intermediate strain conditions can be found by interpolating between two extreme constraints; i.e. CdS/strained-CBTSe and strained-CdS/CBTSe supercell calculations. The valence and conduction band offsets between CBTSe and CdS obtained from bulk core level energies (figure 4) are +1.08 and −0.49 eV, respectively. The proximity of these numbers with supercell calculations presented in table 3 show that the interface dipole and strain contributions do not play a major role in band alignment of the CdS/CBTSe heterojunction. Note that due to their different lattice structures, the band lineups between CdS and non-tetragonal compounds can show larger dependence on interfacial phenomena. This is because larger atomic

redistribution and consequently larger dipole moments can occur at these buffer/absorber interfaces. However, considering the large negative conduction band offsets of all studied Cu_2–II–IV–VI_4 materials with CdS (ranging from −0.49 eV for CBTSe to −1.51 eV for CSGS), different interface orientations and strain contributions are not likely to switch the conduction band offsets from a destructive cliff to a favorable spike conformation. Hence, the main conclusion of previous part—CdS construct harmfull cliff-like conduction band offset with all Cu_2–II–IV–VI_4 compounds—is likely to hold for differently oriented and strained buffer/absorber interfaces.

4. Conclusions

Using first-principles calculations I have studied band discontinuity at buffer/absorber interface of a new class of Cu-based thin film solar cells. The absorber systems considered in this work were Cu_2BaSnS_4, $Cu_2BaSnSe_4$, Cu_2BaGeS_4, $Cu_2BaGeSe_4$, Cu_2SrGeS_4, $Cu_2SrGeSe_4$, Cu_2SrSnS_4, and $Cu_2SrSnSe_4$ and the buffer material was the conventional CdS. The results show that when buffering CBC absorbers with CdS, the conduction band offset adopts a harmful cliff-like conformation, ranging from −0.49 eV for CdS/CBTSe to −1.51 eV for CdS/CSGS heterojunctions. This finding suggests reduced V_{OC} and enhanced interface recombinations, which limit the conversion efficiency of the device. Thus, to further improve the conversion efficiency of solar cells based on this new class of absorber materials, band alignment between CBC absorbers and alternative buffer materials needs to be improved. To investigate the effect of strain, ΔE_c was calculated for three differently strained CdS/CBTSe supercells. I find that coherence with CBTSe substrate (i.e. about 5% contraction of CdS) yields valence and conduction band offsets that are very close to the bulk-intrinsic values. Coherence with CdS (i.e. about 5% expansion of CBTSe), however, increases the ΔE_v and ΔE_c by 70 meV. This reflects the small effects of interface dipole and strain contributions on the band alignment of CdS/CBTSe heterojunction.

Acknowledgments

Special thanks go to Karsten Albe for fruitful discussions and reading the manuscript. This work has been financially supported by Deutsche Forschungsgemeinschaft (DFG) under project No. 414750661. The computing time was provided by Lichtenberg HPC computer resources at TU Darmstadt. The author would like to thank the Hessian Competence Center for High Performance Computing —funded by the Hesse State Ministry of Higher Education, Research and the Arts— for helpful advice.

ORCID iDs

Elaheh Ghorbani https://orcid.org/0000-0002-4037-1602

References

[1] Wu J-L, Hirai Y, Kato T, Sugimoto H and Bermudez V 2018 *VII World Conf. on Photovoltaic Energy Conversion (WCPEC-7)*
[2] Katagiri H, Sasaguchi N, Hando S, Hoshino S, Ohashi J and Yokota T 1997 *Sol. Energy Mater. Sol. Cells* **49** 407
[3] Wang W, Winkler M T, Gunawan O, Gokmen T, Todorov T K, Zhu Y and Mitzi D B 2014 *Adv. Energy Mater.* **4** 1301465
[4] Gunawan O, Gokmen T and Mitzi D B 2014 *J. Appl. Phys.* **116** 084504
[5] Todorov T K, Tang J, Bag S, Gunawan O, Gokmen T, Zhu Y and Mitzi D B 2013 *Adv. Energy Mater.* **3** 34
[6] Gokmen T, Gunawan O, Todorov T K and Mitzi D B 2013 *Appl. Phys. Lett.* **103** 103506
[7] Chen S, Yang J-H, Gong X G, Walsh A and Wei S-H 2010 *Phys. Rev.* B **81** 245204
[8] Shin D, Saparov B, Zhu T, Huhn W P, Blum V and Mitzi D B 2016 *Chem. Mater.* **28** 4771
[9] Xiao Z, Meng W, Li J V and Yan Y 2017 *ACS Energy Lett.* **2** 29–35
[10] Shin D, Zhu T, Huang X, Gunawan O, Blum V and Mitzi D B 2017 *Adv. Mater.* **29** 1606945
[11] Minemoto T, Matsui T, Takakura H, Hamakawa Y, Negami T, Hashimoto Y, Uenoyama T and Kitagawa M 2001 *Sol. Energy Mater. Sol. Cells* **67** 83
[12] Van de Walle C G 1989 *Phys. Rev.* B **39** 1871
[13] Van de Walle C G and Martin R M 1987 *Phys. Rev.* B **35** 8154
[14] Tersoff J 1984 *Phys. Rev.* B **30** 4874
[15] Schleife A, Fuchs F, Rödl C, Furthmüller J and Bechstedt F 2009 *Appl. Phys. Lett.* **94** 012104
[16] Van de Walle C G and Neugebauer J 2003 *Nature* **423** 626
[17] Linderälv C, Lindman A and Erhart P 2018 *J. Phys. Chem. Lett.* **9** 222
[18] Wei S-H and Zunger A 1995 *J. Appl. Phys.* **78** 3846
[19] Wei S-H and Zunger A 1998 *Appl. Phys. Lett.* **72** 2011
[20] Teske C L 1989 *Z. Nat.forsch.* B **34** 386
[21] Tampier M and Johrendt D 2001 *Z. Anorg. Allg. Chem.* **627** 312
[22] Teske C L 1976 *Z. Anorg. Allg. Chem.* **419** 67
[23] Hersh P A 2008 Wide band gap semiconductors and insulators: synthesis, processing and characterization *Dissertation* Oregon State University

[24] Kresse G and Furthmueller J 1996 *Phys. Rev.* B **54** 11169
[25] Kresse G and Furthmueller J 1996 *Comput. Mater. Sci.* **6** 15
[26] Heyd J, Scuseria G E and Ernzerhof M 2003 *J. Chem. Phys.* **118** 8207
[27] Traill R J and Boyle R W 1955 *Am. Mineral.* **40** 555
[28] Adachi S 2012 *The Handbook on Optical Constants of Semiconductors* (Singapore: World Scientific)
[29] Perdew J P, Burke K and Ernzerhof M 1996 *Phys. Rev. Lett.* **77** 3865
[30] Li Y-H, Walsh A, Chen S, Yin W-J, Yang J-H, Li J, Da Silva J L F, Gong X G and Wei S-H 2009 *Appl. Phys. Lett.* **94** 212109
[31] Ghorbani E, Erhart P and Albe K 2019 *Phys. Rev. Mater.* **3** 075401
[32] Chen S, Walsh A, Yang J-H, Gong X G, Sun L, Yang P-X, Chu J-H and Wei S-H 2011 *Phys. Rev.* B **83** 125201
[33] Weinhardt L, Fuchs O, Groß D, Storch G, Umbach E, Dhere N G, Kadam A A, Kulkarni S S and Heske C 2005 *Appl. Phys. Lett.* **86** 062109
[34] Ge J, Koirala P, Grice C R, Roland P J, Yu Y, Tan X, Ellingson R J, Collins R W and Yan Y 2017 *Adv. Energy Mater.* **7** 1601803
[35] Weston L, Tailor H, Krishnaswamy K, Bjaalie L and de Walle C V 2018 *Comput. Mater. Sci.* **151** 174